A Theoretical and Experimental In-Situ Electrochemical Infrared Spectroscopy Study of Adsorbed CO on Pt Dendrimer-Encapsulated Nanoparticles

Journal of The Electrochemical Society, **163** (4) H3061-H3065 (2016)
0013-4651/2016/163(4)/H3061/5/$33.00 © The Electrochemical Society

JES Focus Issue Honoring Allen J. Bard

A Theoretical and Experimental In-Situ Electrochemical Infrared Spectroscopy Study of Adsorbed CO on Pt Dendrimer-Encapsulated Nanoparticles

Rachel M. Anderson,[a,b] Liang Zhang,[a,c] Dongjun Wu,[d,*] Stanko R. Brankovic,[d,] Graeme Henkelman,[a,c] and Richard M. Crooks[a,b,**,z]**

[a]*Department of Chemistry, The University of Texas at Austin, Austin, Texas 78712-1224, USA*
[b]*Texas Materials Institute, The University of Texas at Austin, Austin, Texas 78712-1224, USA*
[c]*Institute for Computational and Engineering Sciences, The University of Texas at Austin, Austin, Texas 78712-1224, USA*
[d]*Department of Electrical and Computer Engineering, University of Houston, Houston, Texas 77204-4005, USA*

We present a combined experimental and theoretical study of CO_{ads} on Pt_{147} dendrimer-encapsulated nanoparticles (DENs). In-situ electrochemical IR spectroscopy reveals an 8 cm^{-1} redshift of the CO_{ads} stretching frequency on Pt_{147} DENs relative to a Pt(111) crystal. This value is in good agreement with the shift calculated by density functional theory. Importantly, the wavenumber shift observed in this study is significantly smaller than has been found previously. We attribute this primarily to the absence of support effects and the narrow size distribution of DENs. The agreement between experiment and theory validates the model nanoparticle system used for the calculations, and this will make it possible to use the CO_{ads} frequency as a probe to study more complex DEN structures and as a descriptor of the catalytic activity of DENs toward reactions such as formic acid oxidation and methanol oxidation.
 [DOI: 10.1149/2.0061604jes]

Manuscript submitted September 1, 2015; revised manuscript received October 19, 2015. Published December 4, 2015. *This paper is part of the JES Focus Issue Honoring Allen J. Bard.*

We are interested in developing a better understanding of how small changes in the structure of nanoparticles in the 1–2 nm size range impact important electrocatalytic reactions like oxygen reduction and CO oxidation. We approach this problem by directly comparing theory and experiments.[1] This is important, because previous results from our groups and others have shown that nanoparticle structures in this size range are dynamic. For example, core@shell nanoparticles are able to invert,[2,3] ligands can drive shape changes,[4] and interactions with a substrate can result in major electronic and shape changes.[5–7]

One effective method for gaining insight into nanoparticle surface structure is to measure changes in the vibrational frequency of adsorbed CO (CO_{ads}) using infrared (IR) spectroscopy.[8,9] Spectroscopic results from single-crystal surface models are relevant for understanding the structure of Pt nanoparticles (PtNPs) having size >4 nm, but for smaller nanoparticles the connection to bulk surfaces is more tenuous.[8] This is because the dominance of discrete facets is reduced, while the contribution of edge and corner sites increases. These latter sites can be identified because they bind CO more strongly, thereby decreasing its stretching frequencies.[8,10]

It has previously been shown that the CO_{ads} frequency decreases as the size of PtNPs supported on carbon (C/PtNP) decreases.[8,11,12] For example, frequency shifts on the order of 20 cm^{-1} have been reported as nanoparticle size decreases from ∼4 nm to ∼2 nm.[8] However, these studies have been carried out on commercial C/PtNP catalysts, which exhibit wide variations in the size and shape of the PtNPs and also effects exerted by the support.[12,13] This in turn makes it difficult to precisely correlate IR spectra to particular nanoparticle structures.

We sought to better understand the interaction between CO and PtNPs by developing a more refined model system that could be directly compared to first principles theory. The model we chose are dendrimer-encapsulated nanoparticles (DENs), which are well-defined materials in the size range of 1–2 nm.[1,14] DENs are synthesized by first complexing metal ions to the interior of the dendrimer, and then adding a reducing agent. This results in nearly monodisperse nanoparticles that are sterically trapped within the dendrimer interior. The size of DENs can be tuned by changing the ratio of metal ions:dendrimer. Another advantage of DENs is that the dendrimer protects the nanoparticles from agglomeration, but it only weakly interacts with the nanoparticle surface.[15] Additionally, the presence of the dendrimer prevents direct contact between the catalyst and the electrode surface, thereby eliminating contributions to the shape or electronic properties of the nanoparticle arising from support interactions. Note, however, that the slight separation between DENs and the electrode surface does not adversely impact electrocatalytic rate measurements.[16,17] Finally, DENs can be attached to electrodes without using Vulcan carbon or Nafion, both of which are in common use and can influence the structural, spectroscopic, and electrochemical properties of nanoparticles.[18–20] For all these reasons, DENs simplify direct comparison of theory and experiment.

In addition to its use as a reporter of nanoparticle structure,[8,21] the binding energy of CO_{ads} is of interest as a descriptor for different catalytic reactions such as CO electrooxidation, formic acid oxidation, and methanol oxidation.[22–26] In the size range of DENs, the corresponding structure can be modeled using density functional theory (DFT) to make predictions about structure and the binding energies of adsorbates.[1]

In the present study, we report in-situ electrochemical IR spectroscopy and cyclic voltammetry (CV) measurements of CO_{ads} on Pt DENs containing an average of 147 atoms (Pt_{147}),[14] and then compare these experimental results to DFT calculations. The key observation is that the frequency of the CO_{ads} stretching mode is shifted by ∼8 cm^{-1} to lower values on Pt_{147} DENs as compared to a bulk Pt(111) single crystal. The corresponding DFT calculations are consistent with this finding. Importantly, the magnitude of this shift is significantly smaller than that previously reported for commercial supported C/PtNPs. We believe the difference between the results obtained using the DENs model and these earlier studies is due to the absence of support effects, a narrower particle-size distribution, and the absence of ligand effects due to the presence of Nafion or other binders.

Experimental

Chemicals.— Sixth-generation, hydroxyl-terminated (G6-OH) poly(amidoamine) (PAMAM) dendrimers in methanol were purchased from Dendritech (Midland, MI). The dendrimer solvent was removed under vacuum, and then the dendrimers were reconstituted in water at a concentration of 100.0 μM. $NaBH_4$ and K_2PtCl_4 were purchased from Sigma-Aldrich, and $CuSO_4$, NaOH, and high-purity

*Electrochemical Society Student Member.
**Electrochemical Society Active Member.
[z]E-mail: crooks@cm.utexas.edu

$HClO_4$ from Fisher Scientific. All solutions were made using deionized (DI) water having a resistivity of >18.2 MΩ · cm (Milli-Q gradient system, Millipore).

Synthesis and characterization of Pt DENs.— The synthesis of Pt DENs by galvanic exchange has been reported previously.[27,28] Briefly,[29] a 10.0 μM solution of G6-OH PAMAM dendrimer was prepared by dilution of a 100.0 μM stock solution. Next, 55 equiv. of $CuSO_4$ were added from a 0.10 M stock solution. The pH was adjusted to ∼7.5 using 0.30 M NaOH, and then the solution was purged with N_2 and stirred for at least 5 min to allow for complexation between Cu^{2+} and the dendrimer. The solution was continuously purged with N_2 for the remainder of the synthesis procedure. $NaBH_4$ was then added from a freshly prepared 0.10 M stock solution, and the solution stirred for at least 5 min.

Excess unreacted BH_4^- was oxidized by adding a four-fold excess (relative to the original equiv. of BH_4^-) of 0.1 M $HClO_4$ and allowing it to react for 5 min (the pH was maintained above 5 with NaOH throughout the synthesis). The pH of the solution was then raised to ∼6.5 so that additional equiv. of Cu^{2+} could be complexed with the dendrimer. This complexation/reduction cycle was repeated twice more to synthesize Cu_{147} DENs (first with 55 equiv. then with 37 equiv.). The pH was lowered to 3.2 and galvanic exchange of Cu for Pt was carried out by adding 147 equiv. of Pt^{2+} (from a freshly prepared 0.10 M stock solution of $PtCl_4^{2-}$) to the Cu DENs solution so that the Pt^{2+}:Cu ratio was 1.0. After reacting for several minutes the N_2 purge was stopped and the pH of the resulting Pt DENs solution was raised to ∼8.5. An aliquot of the DENs solution was diluted to 2.0 μM, and ∼3 μL was pipetted onto a ultra-thin carbon-coated Cu transmission electron microscopy (TEM) grid (Electron Microscopy Sciences, Hatfield, PA), and the grid was allowed to dry in air. A JEOL-2010F TEM operating at 200 kV was used for size analysis of the Pt DENs.

Electrochemistry.— CVs were obtained in a 0.10 M $HClO_4$ electrolyte solution using a 3 mm-diameter glassy carbon (GC) disk electrode, a Au counter electrode, and a Hg/Hg_2SO_4 reference electrode (CH Instruments, Austin, Texas). The latter was calibrated against an eDAQ Hydroflex hydrogen reference electrode. All potentials were converted to, and reported relative to, the reversible hydrogen electrode (RHE) scale. For electrochemical measurements, a CHI 1202B potentiostat (CH Instruments) was used. For CVs the electrolyte solution was purged with either high-purity Ar or CO.

Electrochemical immobilization of DENs.— The GC disk electrode was polished with alumina, rinsed, and then sonicated for ∼2 min in DI water. Next, Pt DENs were immobilized on the GC disk electrode using a previously reported electrochemical procedure.[30] The DEN concentration used for immobilization was 5.0 μM, and three full potential cycles were performed between 0.50 and 1.30 V. After immobilization, the electrode was rinsed with DI water, and then the DEN surfaces were cleaned by cycling the potential 20 times between 0 and 1.3 V in 0.10 M $HClO_4$.

In-situ IR spectroscopy.— For IR measurements, a ∼1 cm × 1 cm GC chip electrode was used. A Cu wire was attached to the back side with conductive Ag paint, and then the entire back and edges of the GC chip were covered with epoxy (to prevent Ag or Cu contamination). The Cu wire was threaded through a glass rod to provide stability in the electrochemical cell. Electrochemical immobilization of DENs and subsequent cleaning cycles were carried out for the GC chip electrode as previously described for the GC disk electrode. The cell for in-situ IR spectroelectrochemical measurements, described previously,[31] consisted of a ZnSe hemisphere serving as the attenuated total reflectance (ATR) window and cell bottom, and a Teflon body. The spectroelectrochemical cell[32] was filled with CO-saturated 0.10 M $HClO_4$ and outfitted with a Pt counter electrode and a saturated calomel reference electrode. The GC chip working electrode was positioned and secured firmly against the top of the ZnSe crystal (at the bottom of the cell). A potential of 0.05 V was applied, the spectroelectrochemical cell lid closed, and the entire compartment housing the spectroelectrochemical cell and detector was closed and purged with dry compressed air for ∼1 h.

IR spectra were obtained using a Nicolet 6700 FTIR having an MCT-A liquid nitrogen-cooled detector. A spectrum of CO_{ads} was obtained at 0.05 V immediately after purging the system with dry air. Next the potential was stepped to 0.96 V to oxidize and desorb CO_{ads}, and then a reference spectrum was obtained. Both spectra were acquired at 8 cm^{-1} resolution and 1024 scans were co-added. The two single-beam spectra were subtracted and normalized to isolate the signal due to the CO_{ads} using the following equation: $-\Delta R/R = -(R - R_{ref})/R_{ref})$. Here, R is the reflectance in the presence of CO_{ads}, and R_{ref} is the reflectance in the absence of CO_{ads}. The spectrum of CO_{ads} on Pt_{147} DENs is plotted as $\Delta R/R$ to correct for the peak inversion observed with respect to the Pt(111) electrode. Peak inversion has been previously reported for thin noble metal catalyst layers on GC electrodes.[33,34]

In addition to Pt DENs, spectra of CO_{ads} were also obtained from a Pt(111) single crystal. The Pt crystal was prepared using a standard procedure commonly reported in the literature.[35] The Pt electrode was then immediately placed into the in-situ IR spectrometer set-up, and then the same procedure used for the Pt_{147} DENs was followed for IR experiments.

Computational methods.— DFT calculations were performed using the Vienna ab initio simulation package.[36,37] Core electrons were described using the projector-augmented wave method.[38,39] Kohn-Sham single-electron wave functions were expanded in a plane-wave basis with a kinetic energy cutoff of 280 eV to describe the valence electrons. The generalized gradient approximation (GGA) using the Perdew-Wang 91 functional was chosen to evaluate the exchange-correlation energy.[40] All atoms in the nanoparticle were allowed to relax; geometries were considered optimized when the force on each atom was <0.005 eV/Å. Convergence was checked by increasing the energy cutoff to 400 eV, and the CO binding energy on a Pt 147-atom nanoparticle was found to change by only 1 meV (<0.1%). Theoretical IR spectra were calculated based on fully optimized structures using Porezag's scheme as implemented in the Atomic Simulation Environment (ASE).[41]

Pt_{147} was modeled as a 147-atom face-centered cubic (FCC) cuboctahedron nanoparticle in a 3 nm cubic cell, which ensures a sufficient vacuum gap between periodic images. The IR spectrum of the Pt(111) surface was calculated using as a (4 × 4) Pt(111) slab with 4 atomic layers and 14 Å of vacuum. The Brillouin zone was sampled using a 3 × 3 × 1 Monkhorst-Pack k-point mesh for Pt(111) and the Gamma point for Pt_{147}.[42] A (2 × 2) Pt(111) slab model with (5 × 5 × 1) k-point mesh was used to estimate the coverage dependence of the CO atop stretching frequency. The CO atop stretching frequency was calculated at a CO coverage of 0.25, 0.5, 0.75 and 1.0. The Hessian matrix was determined using density functional perturbation theory.

Results and Discussion

Synthesis and immobilization of Pt_{147} DENs.— Pt_{147} DENs were prepared as follows. First, as described in detail in the Experimental section, Cu_{147} DENs were prepared by sequential complexation and reduction steps. Second, the Cu_{147} DENs were reacted with Pt^{2+} to yield Pt_{147} DENs via a process known as galvanic exchange.[27,43] Figure 1 shows a TEM micrograph of the resulting Pt_{147} DENs as well as a size-distribution histogram. The average diameter for Pt_{147} is 1.7 ± 0.2 nm, which is consistent with previous reports[29,44,45] and with the calculated diameter of 1.6 nm.[45] The close proximity of the DENs in Figure 1a suggests some interaction between the dendrimers upon drying on the carbon TEM grid, but these DENs are stable in solution and exhibit no evidence of agglomeration. Note that the diameter of each DEN was measured by assuming each to be a separate, spherical nanoparticle.

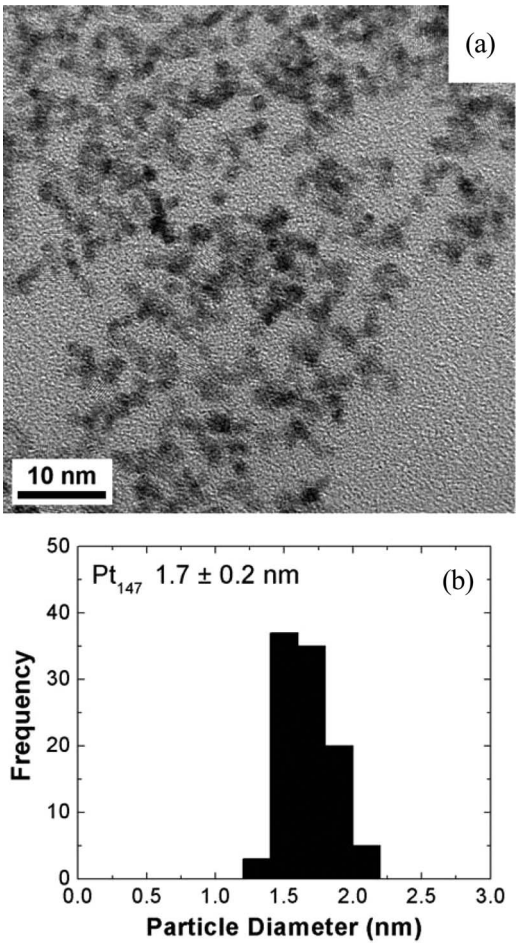

Figure 1. (a) TEM image of Pt_{147} DENs. (b) Size-distribution histogram of Pt_{147} DENs showing an average diameter of 1.7 ± 0.2 nm.

The Pt_{147} DENs were immobilized onto a GC disk electrode using a previously reported electrochemical immobilization method[30] that is briefly summarized in the Experimental section. Although surrounded by dendrimers and not in direct electrical contact with the underlying electrode, the Pt_{147} nanoparticles are in electrochemical equilibrium with the electrode surface.[16,17] The electrochemically active surface area of the Pt_{147} DENs was determined by integrating the hydride adsorption region of CVs and found to be 0.058 ± 0.005 cm^2. This corresponds to a coverage of ~1.7 monolayer of close-packed dendrimers, which is consistent with previous reports.[46,47] This calculation is approximate and relies on several assumptions that we have outlined previously.[45] These include the diameter of the nanoparticles, the size of the adsorbed dendrimers, and the roughness of the electrode surface.

CO oxidation.— Electrochemical experiments were performed to determine the CO stripping peak potential. The electrode was prepared as described in the Experimental section, and then moved to a fresh solution of CO-purged 0.10 M $HClO_4$. Next, the potential was stepped to 0.05 V, and after 5 min the purge gas was changed to Ar for an additional 5 min. This results in adsorption of CO onto the Pt surface and removal of bulk CO from solution. As shown in Figure 2, the electrode potential was then cycled from 0.05 V to 1.30 V and then back to 0 V twice. Notice that the current axis in Figure 2 is normalized to the electrochemically active surface area of Pt.

During the first positive-going scan, which begins at 0.050 V, CO_{ads} is oxidized to CO_2 at 0.92 ± 0.03 V. At higher potentials, the Pt_{147} DEN surface oxidizes, and upon scan reversal a PtO_x reduction peak is present at ~0.68 V. As the potential continues to decrease, the

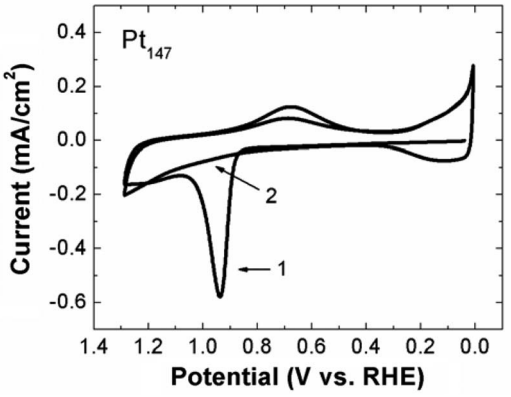

Figure 2. CV of Pt_{147} DENs showing the oxidation of a monolayer of CO_{ads} in 0.10 M $HClO_4$. The scan began at 0.05 V and proceeded in a positive direction at 50 mV/s. The current axis is normalized to the electrochemically active surface area of Pt.

onset of hydride adsorption is observed at ~0.30 V on the now naked Pt surface. At the beginning of the second cycle, hydride desorption features are observed due to the absence of CO_{ads}, but the characteristic CO_{ads} oxidation peak is not present. The remainder of the second scan very nearly overlays the first scan. Integration of the CO_{ads} oxidation peak reveals the ratio of these charges (H_{ads}:CO_{ads}) is 0.38 ± 0.05, which is consistent with previous reports of more than a monolayer of CO_{ads} present on particles ≤2 nm.[8,45,48] The key point, however, is that the procedure we developed to immobilize Pt_{147} DENs on the carbon electrode, saturate their surfaces with CO, and then remove CO_{ads} is effective. Accordingly, we are prepared to examine the CO_{ads} vibrational frequency using in-situ IR spectroscopy.

In-situ electrochemical IR.— The technique of subtractively normalized interfacial Fourier transform infrared spectroscopy (SNIFTIRS) has been used extensively to study CO_{ads} on bulk (usually single crystal) metal surfaces,[49,50] but there are few reports of its use for understanding CO_{ads} on nanoparticles having diameters ≤ 2 nm.[8,9,11,12,51] Note, however, that in-situ IR has been used to study CO_{ads} on DENs in the gas phase and in solution.[52]

To ensure that we are able to duplicate literature procedures and for comparative purposes, we first obtained a spectrum of CO_{ads} on a Pt(111) single crystal prepared as described in the Experimental section. The IR spectrum was obtained as follows. First, a spectrum was obtained with the electrode potential held at 0.050 V, which means that it was covered with CO_{ads}. A second spectrum was then measured after stepping the potential to 0.96 V, where CO_{ads} is oxidized to soluble CO_2 and hence removed from the electrode surface. These two spectra were processed as described in the Experimental section, and the result is shown in Figure 3a. The CO_{ads} stretching band is very strong, narrow, and centered at 2066 cm^{-1}. These features are consistent with previously reported observations.[53-55]

Following the same procedure used for the Pt(111) single crystal, we next obtained an IR spectrum of CO_{ads} on the Pt_{147} DEN-modified GC electrode (Figure 3b). The resulting peak is broader, less intense, and shifted by 8 cm^{-1} to 2058 cm^{-1}. These features are similar to those previously reported for Pt_{147} DENs in an ethanol solution but not under potential control (CO_{ads} peak centered at 2063 cm^{-1}).[52]

The direction of the CO_{ads} peak shift between Pt(111) and Pt_{147} DENs (Figure 3) is in accord with prior literature reports of a redshift with decreasing size of nanoparticles <4 nm in diameter. However, its magnitude (8 cm^{-1}) is quite different. For example, Arenaz et al. observed a value of 2052 cm^{-1} for ~2.0−2.5 nm PtNPs supported on carbon (C/PtNPs) and 2049 cm^{-1} for ~1−1.5 nm C/PtNPs (shifts of 14 and 17 cm^{-1}, respectively, compared to Pt(111)) using the same applied electrode potential and a Nafion binding layer.[11] Park et al. observed a value of ~2042 cm^{-1} (a shift of 24 cm^{-1} compared to

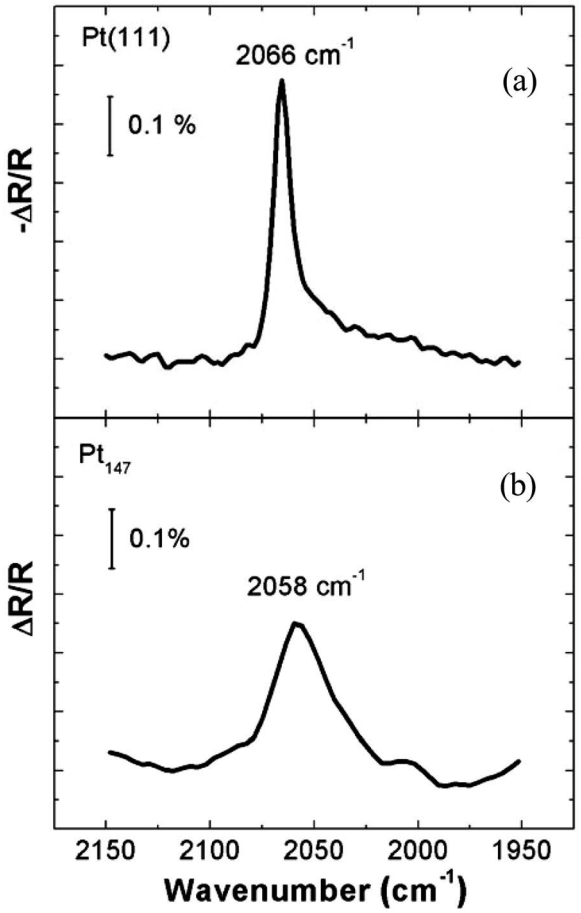

Figure 3. IR spectra of CO_{ads} on (a) Pt(111) and (b) Pt_{147} DENs. The spectrum of CO_{ads} was acquired at 0.05 V, and a reference spectrum (no CO_{ads}) was collected at 0.96 V. The electrolyte solution was 0.10 M $HClO_4$. A total of 1024 scans were collected at 8 cm^{-1} resolution.

Pt(111)) for 2.0 nm C/PtNPs (the size distribution was not specified) using an applied potential of 0 V vs. RHE.[8] The difference in the magnitude of these reported shifts and those represented in Figure 3 is most likely a consequence of support interactions present in the earlier studies. In contrast, DENs are unsupported nanoparticles in the sense that there is no direct contact between the DENs and the electrode surface. Previous nuclear magnetic resonance (NMR) studies have reported on the effect of the interaction between the conductive carbon support and PtNPs on the CO_{ads} frequency.[12,13] A stronger electronic effect was observed on smaller nanoparticles, and suggested that shifts in frequency with size are dominated by this strong support interaction.[12] DENs are not subject to such strong interactions, and this could be an explanation for why a smaller shift is observed here. For example, the higher symmetry of DENs, which are undistorted by the underlying substrate, undoubtedly exhibit a different degree of surface strain compared to Pt nanoparticles in direct contact with the electrode.

DFT calculations.— DFT was used to better understand the observed IR frequency shift between Pt(111) and Pt_{147}. The Pt(111) system was investigated first. A monolayer of CO in the atop binding configuration was used to generate the IR spectrum for Pt(111) in Figure 4 (black trace). The coverage of CO on Pt(111), however, has been experimentally determined to be 0.75.[54] Figure 5 shows the dependence of the average CO frequency as a function of coverage. There is a difference in the CO atop stretching frequency on the Pt slab at a coverage of 1.0 between Figures 4 and 5, and we attribute this small shift to the numerical differences between the two frequency calculation methods used. For the IR spectrum calculation in Figure 4, the Hessian matrix is determined by finite difference, while in Figure 5 the Hessian matrix was calculated by density functional perturbation theory. However, we believe that the magnitude of the frequency shift as a function of coverage is robust with respect to the computational implementation of the frequency calculation. The key point is that a shift of ~20 cm^{-1} occurs between 1.0 and 0.75 monolayer coverage. As such, the calculated value (2072 cm^{-1}) is shifted by this 20 cm^{-1} to yield a value of 2052 cm^{-1} for Pt(111).

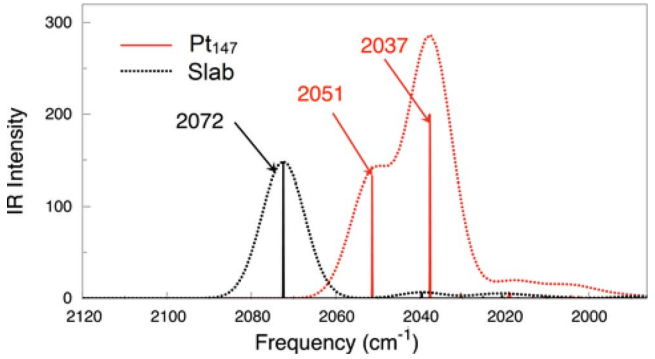

Figure 4. Calculated vibrational spectra of CO_{ads} on Pt(111) and Pt_{147} DENs.

Next, the Pt_{147} model was constructed. A monolayer of atop CO was added to the Pt_{147} structure and the CO stretching frequencies computed. In this case, single-monolayer coverage of CO is consistent with the experimental data. Pt_{147} can accommodate more CO_{ads} as compared to the Pt(111) system because of the high curvature of the nanoparticle surface, which reduces CO-CO repulsion. It was observed in our calculations that the CO binding on Pt(111) weakened from −1.51 eV to 0.10 eV with an increase of CO coverage from 1/16 of a monolayer to 1 monolayer on Pt(111). The positive CO binding energy of 1 monolayer of CO on Pt(111) also indicates the difficulty of achieving such a high coverage. However, CO binding only changes from −1.94 eV to −1.44 eV on the (111) facet of Pt_{147} with an increase in coverage from the bare nanoparticle to 1 monolayer.

Figure 4 (red trace) shows the calculated IR spectrum, with two main populations centered at 2051 cm^{-1} and 2037 cm^{-1} with an average value of 2041 cm^{-1}. The peak splitting is due to coupling between the CO molecules resulting in in-phase and out-of-phase CO stretching modes across the entire nanoparticle. One important difference to

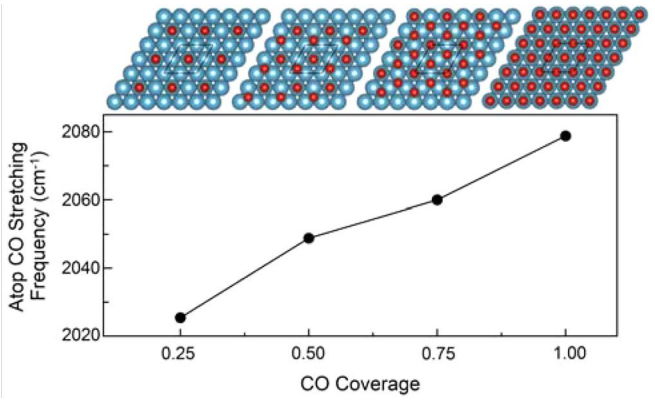

Figure 5. Plot of the calculated trend of frequency of atop CO_{ads} vs. the fractional coverage on a Pt(111) surface. The pictures above the plot show the structure of CO adsorbed on the Pt(111) surface at each coverage. Cyan, brown, and red indicate Pt, C and O atoms. The (2 × 2) cell used is shown by the black line. The CO molecules were placed at their lowest energy sites. At 0.25 coverage, one CO was placed at an atop site; at 0.5 one CO is on an atop and the second on an HCP site; at 0.75 the sites occupied are atop, HCP, and FCC; at 1.0 each atop site has a bound CO molecule.

note between experiment and theory is that the applied electrochemical potential is not taken into account in the DFT calculations, so we are only interested in comparing shifts and not absolute frequency values. In terms of correlating experiment and theory, we begin by looking at the observed experimental shift between the Pt(111) and Pt_{147} system, which was found to be 8 cm^{-1}. This is close in magnitude to the difference of ∼11 cm^{-1} observed for the theoretical spectra of CO on Pt(111) and the Pt_{147} (2052 cm^{-1} for Pt(111) at a coverage of 0.75, and 2041 cm^{-1} for Pt_{147} DENs). The broadening of the experimental Pt_{147} IR peak as compared to the single crystal Pt(111) peak is also observed in the theoretical spectra, but with the 8 cm^{-1} resolution used here it is difficult to interpret more from the shape of the experimental peaks.

From the good agreement between experiment and theory in the direction and magnitude of the shift between Pt DENs and the Pt(111) crystal, our model system of the Pt_{147} DEN is corroborated. As this is a complicated electrochemical system involving potential control and other factors, it is valuable to know that relative shifts observed theoretically for important reactant descriptors (such as CO_{ads}) are valid for application to experimental systems.

Conclusions

We have presented a combined experimental and theoretical study of CO_{ads} on Pt_{147} DENs. IR spectroscopy revealed an 8 cm^{-1} redshift of the CO_{ads} stretching frequency on Pt_{147} DENs relative to a Pt(111) crystal. This value is in good agreement with the shift calculated using theoretical model systems. Importantly, the wavenumber shift observed in our study is significantly smaller than has been found previously. We attribute this primarily to the absence of support effects and the narrow size distribution of DENs. The agreement between experiment and theory validates the model nanoparticle system used for the calculations, and this will make it possible to use the CO_{ads} frequency as a probe to study more complex DEN structures and as a descriptor of the catalytic activity of DENs toward reactions such as formic acid oxidation and methanol oxidation.

Acknowledgments

We acknowledge support from the Chemical Sciences, Geosciences, and Biosciences Division, Office of Basic Energy Sciences, Office of Science, U. S. Department of Energy (Contract: DE-FG02-13ER16428). We also thank the Robert A. Welch Foundation (grant Nos. F-0032 and F-1841) for sustained support of our research program. S.R.B. and D.W. gratefully acknowledge support from the National Science Foundation (grant no. 0955922).

References

1. R. M. Anderson, D. F. Yancey, L. Zhang, S. T. Chill, G. Henkelman, and R. M. Crooks, *Acc. Chem. Res.*, **48**, 1351 (2015).
2. M. G. Weir, M. R. Knecht, A. I. Frenkel, and R. M. Crooks, *Langmuir*, **26**, 1137 (2010).
3. R. M. Anderson, L. Zhang, J. A. Loussaert, A. I. Frenkel, G. Henkelman, and R. M. Crooks, *ACS Nano*, **7**, 9345 (2013).
4. D. F. Yancey, S. T. Chill, L. Zhang, A. I. Frenkel, G. Henkelman, and R. M. Crooks, *Chem. Sci.*, **4**, 2912 (2013).
5. M.-C. Daniel and D. Astruc, *Chem. Rev.*, **104**, 293 (2004).
6. S. Schauermann, N. Nilius, S. Shaikhutdinov, and H.-J. Freund, *Acc. Chem. Res.*, **46**, 1673 (2013).
7. B. R. Cuenya, *Thin Solid Films*, **518**, 3127 (2010).
8. S. Park, S. A. Wasileski, and M. J. Weaver, *J. Phys. Chem. B*, **105**, 9719 (2001).
9. K. J. J. Mayrhofer, M. Arenz, B. B. Blizanac, V. Stamenkovic, P. N. Ross, and N. M. Markovic, *Electrochim. Acta*, **50**, 5144 (2005).
10. M. J. Kappers and J. H. van der Maas, *Catal. Lett.*, **10**, 365 (1991).
11. M. Arenz, K. J. J. Mayrhofer, V. Stamenkovic, B. B. Blizanac, T. Tomoyuki, P. N. Ross, and N. M. Markovic, *J. Am. Chem. Soc.*, **127**, 6819 (2005).
12. C. Rice, Y. Tong, E. Oldfield, A. Wieckowski, F. Hahn, F. Gloaguen, J.-M. Léger, and C. Lamy, *J. Phys. Chem. B*, **104**, 5803 (2000).
13. Y. Tong, C. Rice, A. Wieckowski, and E. Oldfield, *J. Am. Chem. Soc.*, **122**, 1123 (2000).
14. V. S. Myers, M. G. Weir, E. V. Carino, D. F. Yancey, S. Pande, and R. M. Crooks, *Chem. Sci.*, **2**, 1632 (2011).
15. M. V. Gomez, J. Guerra, A. H. Velders, and R. M. Crooks, *J. Am. Chem. Soc.*, **131**, 341 (2009).
16. J.-N. Chazalviel and P. Allongue, *J. Am. Chem. Soc.*, **133**, 762 (2011).
17. A. Barfidokht, S. Ciampi, E. Luais, N. Darwish, and J. J. Gooding, *Anal. Chem.*, **85**, 1073 (2013).
18. S. Sharma and B. G. Pollet, *J. Power Sources*, **208**, 96 (2012).
19. M. S. McGovern, E. C. Garnett, C. Rice, R. I. Masel, and A. Wieckowski, *J. Power Sources*, **115**, 35 (2003).
20. D. Malevich, J. Li, M. K. Chung, C. McLaughlin, M. Schlaf, and J. Lipkowski, *J. Solid State Electrochem.*, **9**, 267 (2005).
21. C. Gumeci, A. Marathe, R. L. Behrens, J. Chaudhuri, and C. Korzeniewski, *J. Phys. Chem. C*, **118**, 14433 (2014).
22. S. W. Lee, S. Chen, W. Sheng, N. Yabuuchi, Y.-T. Kim, T. Mitani, E. Vescovo, and Y. Shao-Horn, *J. Am. Chem. Soc.*, **131**, 15669 (2009).
23. S. Park, Y. Xie, and M. J. Weaver, *Langmuir*, **18**, 5792 (2002).
24. M. Neurock, M. Janik, and A. Wieckowski, *Faraday Discuss.*, **140**, 363 (2008).
25. R. Iyyamperumal, L. Zhang, G. Henkelman, and R. M. Crooks, *J. Am. Chem. Soc.*, **135**, 5521 (2013).
26. N. Kristian, Y. Yan, and X. Wang, *Chem. Commun.*, 353 (2008).
27. M. Zhao and R. M. Crooks, *Chem. Mater.*, **11**, 3379 (1999).
28. S. Pande, M. G. Weir, B. A. Zaccheo, and R. M. Crooks, *New J. Chem.*, **35**, 2054 (2011).
29. R. M. Anderson, D. F. Yancey, J. A. Loussaert, and R. M. Crooks, *Langmuir*, **30**, 15009 (2014).
30. H. Ye and R. M. Crooks, *J. Am. Chem. Soc.*, **127**, 4930 (2005).
31. N. S. Marinković, M. Hecht, J. S. Loring, and W. R. Fawcett, *Electrochim. Acta*, **41**, 641 (1996).
32. R. Loukrakpam, Q. Yuan, V. Petkov, L. Gan, S. Rudi, R. Yang, Y. Huang, S. R. Brankovic, and P. Strasser, *Phys. Chem. Chem. Phys.*, **16**, 18866 (2014).
33. R. Ortiz, A. Cuesta, O. P. Márquez, J. Márquez, J. A. Méndez, and C. Gutiérrez, *J. Electroanal. Chem.*, **465**, 234 (1999).
34. G.-Q. Lu, S.-G. Sun, S.-P. Chen, and L.-R. Cai, *J. Electroanal. Chem.*, **421**, 19 (1997).
35. J. Clavilier, R. Faure, G. Guinet, and R. Durand, *J. Electroanal. Chem. Interfacial Electrochem.*, **107**, 205 (1980).
36. G. Kresse, *Phys. Rev. B*, **62**, 8295 (2000).
37. G. Kresse and J. Hafner, *Surf. Sci.*, **459**, 287 (2000).
38. P. E. Blöchl, *Phys. Rev. B*, **50**, 17953 (1994).
39. G. Kresse and D. Joubert, *Phys. Rev. B*, **59**, 1758 (1999).
40. J. P. Perdew and Y. Wang, *Phys. Rev. B*, **45**, 13244 (1992).
41. D. Porezag and M. R. Pederson, *Phys. Rev. B*, **54**, 7830 (1996).
42. H. J. Monkhorst and J. D. Pack, *Phys. Rev. B*, **13**, 5188 (1976).
43. S. R. Brankovic, J. X. Wang, and R. R. Adzic, *Surf. Sci.*, **474**, L173 (2001).
44. M. R. Knecht, M. G. Weir, V. S. Myers, W. D. Pyrz, H. Ye, V. Petkov, D. J. Buttrey, A. I. Frenkel, and R. M. Crooks, *Chem. Mater.*, **20**, 5218 (2008).
45. H. Ye, J. A. Crooks, and R. M. Crooks, *Langmuir*, **23**, 11901 (2007).
46. E. V. Carino and R. M. Crooks, *Langmuir*, **27**, 4227 (2011).
47. D. F. Yancey, E. V. Carino, and R. M. Crooks, *J. Am. Chem. Soc.*, **132**, 10988 (2010).
48. F. Maillard, M. Eikerling, O. V. Cherstiouk, S. Schreier, E. Savinova, and U. Stimming, *Faraday Discuss.*, **125**, 357 (2004).
49. S. R. Brankovic, J. X. Wang, and R. R. Adžić, *Electrochem. Solid-State Lett.*, **4**, A217 (2001).
50. C. Korzeniewski, *Crit. Rev. Anal. Chem.*, **27**, 81 (1997).
51. F. Maillard, E. R. Savinova, P. A. Simonov, V. I. Zaikovskii, and U. Stimming, *J. Phys. Chem. B*, **108**, 17893 (2004).
52. M. A. Albiter, R. M. Crooks, and F. Zaera, *J. Phys. Chem. Lett.*, **1**, 38 (2010).
53. N. M. Marković, C. A. Lucas, A. Rodes, V. Stamenković, and P. N. Ross, *Surf. Sci.*, **499**, L149 (2002).
54. I. Villegas and M. J. Weaver, *J. Chem. Phys.*, **101**, 1648 (1994).
55. A. López-Cudero, A. Cuesta, and C. Gutiérrez, *J. Electroanal. Chem.*, **579**, 1 (2005).